International Information and Engineering Technology Association
Advancing the World of Information and Engineering

Enhanced Prosthesis Control Through Improved Shoulder Girdle Motion Recognition Using Time-Dependent Power Spectrum Descriptors and Long Short-Term Memory

Huda M. Radha[1*], Alia K. Abdul Hassan[2], Ali H. Al-Timemy[3]

[1] Computer Science Department, Science College, Baghdad University, Baghdad 964, Iraq
[2] Computer Sciences Department, University of Technology, Baghdad 964, Iraq
[3] Biomedical Engineering Department, Al-Khwarizmi College of Engineering, Baghdad University, Baghdad 964, Iraq

Corresponding Author Email: huda.rada@sc.uobaghdad.edu.iq

ABSTRACT

Surface electromyography (sEMG) and accelerometer (Acc) signals play crucial roles in controlling prosthetic and upper limb orthotic devices, as well as in assessing electrical muscle activity for various biomedical engineering and rehabilitation applications. In this study, an advanced discrimination system is proposed for the identification of seven distinct shoulder girdle motions, aimed at improving prosthesis control. Feature extraction from Time-Dependent Power Spectrum Descriptors (TD-PSD) is employed to enhance motion recognition. Subsequently, the Spectral Regression (SR) method is utilized to reduce the dimensionality of the extracted features. A comparative analysis is conducted between the Linear Discriminant Analysis (LDA) classifier and a Deep Learning (DL) approach employing the Long Short-Term Memory (LSTM) classifier to evaluate the classification accuracy of the different motions. Experimental results demonstrate that the LSTM classifier outperforms the LDA-based approach in gesture recognition, thereby offering a more effective solution for prosthesis control.

1. INTRODUCTION

Human forearm loss severely restricts daily activities and interactions for people who have undergone upper limb amputations [1]. Myoelectric control can be used to restore the ability to interact with the real world [2, 3] by deriving control instructions for powered upper-limb prosthetics from electromyogram (EMG) data produced by human muscles. Using a pattern recognition framework, the obtained EMG signals are typically classified into one of many predefined sets of forearm movements [4]. Furthermore, due to the complexity of detecting phantom movement in the absence of a stump and biosensor-associated limitations such as sensor placement and difficulty using wearables, the design space for shoulder disarticulation prostheses is limited [5]. Additional insight on prosthesis sensors and control architectures can be found in survey papers by Nsugbe [6] and Fougner et al. [7]. Machine learning algorithms and approaches have been presented as a superior method to conventional methods for improving system performance in signal recognition and have been used to develop novel bioelectrical signal processing techniques and methods for motion pattern recognition [8]. However, for hand gesture and elbow motion pattern detection, these machine learning approaches typically employ multi-channel EMG signal processing and pattern recognition algorithms [9]. Parajuli et al. [10] addressed major challenges in contemporary artificial intelligence dynamics and concepts arising from the EMG-PR prosthetic control approach. Factors examined included changes in contractile muscle forces, subject movement, and electrode displacement to determine their effects on prosthesis design. Muscle

contraction force and subject movement, for example, were found to detrimentally impact EMG-Pattern Recognition (PR)-enabled prosthetic performance, with error values of approximately 17.00% and 8.98%, respectively. The authors therefore focused their investigations on the most significant issues and best practices in intelligent prosthetics [10]. According to Moradi and Boostani, a feature set should have the highest possible class separability, be as robust as practical in a noisy environment, and be low in complexity [11]. This was achieved by developing an EMG-based controller using various temporal and spectral feature extraction techniques [4, 12]. Hudgins et al. [4], among the first to examine time-domain features in myoelectric control, demonstrated the usefulness of basic features such as mean absolute value, slope sign changes, zero crossings, mean absolute value slope, and waveform length. Additionally, techniques such as Root-Mean Square, Willison amplitude, Integral Absolute Value, log detectors, V-order, and Variance have been employed by many research groups [12, 13].

One benefit of using time-domain features is the simplicity of feature extraction. While features extracted using time-domain methods have shown success and are suitable for real-time control, there is still debate in the literature over whether pattern recognition results using these feature vectors provide high classification accuracies [13]. This stems from the fact that such approaches assume the EMG signal to be stationary despite its non-stationary nature [14]. As a result, researchers' attention turned to spectral moments and features derived from spectral parameters, as well as autoregressive models [15]. Examples of time-frequency representations include short-time Fourier transforms, wavelet transforms, continuous

wavelet transforms, wavelet packet transforms, Wigner-Ville distributions, and Choi-Williams distributions [16, 17].

Pattern recognition (PR) is more robust to force fluctuations when employing the Time-Dependent Power Spectrum Descriptor (TD-PSD) with force magnitude-based training compared to most dimensionality reduction techniques [18]. Al-Timemy et al. presented a study to develop a technique with minimal error rates and faster response times than other test-based methods. EMG signals were collected from a group of amputees. The study found that TD-PSD could be a suitable alternative to feature extraction (FE) approaches in PR-based implementations [19].

Khushaba et al. [20] proposed a spatiotemporal descriptor for TSDs that accepted a set of EMG features gathered from various healthy and amputated limbs on high-density (HD) electrode grids to implement multiple degrees of freedom (finger and hand movements). Sharba et al. [21], on the other hand, used a set of widely used EMG sensors that monitor electrical signals associated with contractile muscle activity and other data acquisition methods. Accelerometers (Acc) were used to quantify skeletal movements resulting from movements of specific shoulder gestures as well as low-frequency displacements resulting from anatomical contractions.

Modern artificial intelligence techniques such as Deep Learning and unsupervised learning are applied in this field. Deep Learning can be thought of as artificial intelligence functions that are synergistic with human ways of thinking [22]. Recurrent neural networks (RNNs) are interconnected artificial networks that use sequentially or time-dependent data where the input to the current layer is the output of the previous layer. However, standard recurrent networks struggle with vanishing gradients caused by the steady decline of gradient backpropagation, making learning long data sequences difficult.

Long Short-Term Memory (LSTM) units provide a solution to these problems. They solve this by storing long time input signal steps during firing time and are resilient to arbitrary data input [23]. Qiao and Li [24] presented a pattern recognition method for an EMG signal-based LSTM model with PCA dimensionality reduction. They compared it to well-known pattern recognition methods such as SVM and random forest algorithms. They found that the PCA-LSTM approach outperformed other algorithms in terms of recognition rate and efficiency. It solves the "curse of dimensionality" problem and improves EMG signal recognition rates, laying the foundation for practical implementation of the algorithm model. Dao [25] used transfer learning to build and test an LSTM network for skeletal muscle force predictions. Also, with the help of LSTM, Chen et al. [26] demonstrated how their continuous estimation model for upper limb joint angles increased estimation accuracy.

A myoelectric prosthetic arm might be able to conduct a variety of shoulder motions while minimizing cognitive load if it has the ability to recognize shoulder motions and is combined with therapy-related neuro muscle programming. The following are the significant contribution of the study, which have been highlighted and summarized:

1). by taking Time Dependent Power Spectrum Descriptors (TDP-SD) to extract features which Combines six features such as Roots square zero-ordered moments ($\overline{m}_0$), Root squared 2nd-order moment ($\overline{m}_2$) and 4th-order moment ($\overline{m}_4$), Sparseness, Irregularity Factor (IF), Waveform Length Ratio (WL) to extract 48-dimensional feature vectors from each

subject (amputee or healthy person).

2). we explore the effects of LSTM and LDA classifiers on analysis of testing error.

2. METHODOLOGY

This work used a variety of approaches and strategies to extract features from bio-signals, reduce the dimensionality of extracted features, and estimate the motion class. Below is a brief description of these strategies and procedures.

2.1 Timely-Depend Powers Spectrums Descriptor (TD-PSDs) concept

The EMG signal during a specific iteration could be described as a relationship of frequencies $X[k]$ using Discrete-Fourier-transformation (DFT) with the availability of the processed item of the EMGs input indicated as $x[j]$, of j=1, 2 ...N, N represents the length and a sampler frequencies (fs)Hz. The first step in the feature extraction procedure is to remember Parsval's theory, which asserts that the summation of the squares of a relationship and its transform is identical [19].

$$\sum_{j=0}^{N-1}|x[j]|^2 = \frac{1}{N}\sum_{k=0}^{N-1}|X[k]X^*[k]| = \sum_{k=0}^{N-1}p[k] \qquad (1)$$

where, in the equation above, $p[k]$ stands for the phase excluded power spectrum. Using [k] multiplied by the $X[k]$ conjugate and divided by N, the frequency index is determined, where $p[k]$ denotes the phase-excluded power spectrograph, this indicates that $X[k]$ has a conjugate, $X^*[k]$, that is divided by N, compounded by k, and frequency index. The Fourier transformation's entire definition of frequency is frequently recognized as being symmetrically based in terms of nullified frequencies; that is, it contains comparable parts extensive to both positive and negative frequencies [27]. This symmetry is absent throughout the range, considering both positively and negatively sampled signals. Admittance to spectrum powers in the time-space is yet restricted. As indicated by the idea of a single-minute m of the request n $p[k]$ of power spectrum thickness, all unpredictable minutes are likewise zero by the recurrence dispersion model's measurable technique [19].

$$m_n = \sum_{k=0}^{N-1}k^n p[k] \qquad (2)$$

For non-zero values of n, the Fourier transform's time-differentiation property is used, and when n is zero, Parseval's theorem in Eq. (1) is applied. The spectrum multiplied by k raised to the nth power equals the nth derivative of a function in the time domain denoted as Δ^n designated as for discrete-time signals, according to this condition [19].

$$F[\Delta^n x[j]] = k^n X[k] \qquad (3)$$

To that end, the following features are defined in this work, as shown in Figure 1.

The scheme in Figure 1 states that the specified six attributes are first retrieved from each EMG record x and then formed into a vector a= [a1... a6]. Then, a component vector a (as per EMG records) and a component vector b are obtained by subtracting an extra component vector b= [b1... b6] from a

logarithmically weighted variant log (x2) (from a nonlinear weighted rendition of the EMG record), each having six parts. The TD-PSD features used in this study are as follows:
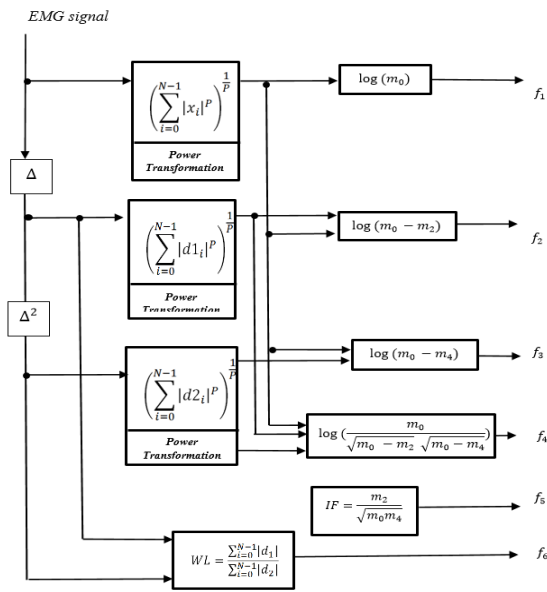
Figure 1. Block diagram for TD-PSD feature extraction process

a)   Root squared zero-order moment ($\overline{m}_0$):

The following feature displays the overall power in the frequency domain, or just the force of muscle contraction.

$$\overline{m}_0 = \sqrt{\sum_{j=0}^{N-1} x[j]^2} \qquad (4)$$

To normalize the resultant zero-order moments, add up all of the zero-order moments from all channels.

b)   Second and fourth-order root squared moments:

The second moment can be thought of as a power, but according to Hjorth [27], it is a modified spectrum $k^2 p[k]$, which corresponds to a frequency function [19].

$$\overline{m}_2 = \sqrt{\sum_{k=0}^{N-1} k^2 P[k]} = \sqrt{\frac{1}{N}\sum_{k=0}^{N-1}(kX[k])^2} = \sqrt{\sum_{j=0}^{N-1}(\Delta x[j])^2} \qquad (5)$$

A repetition of this procedure gives the moment.

$$\overline{m}_4 = \sqrt{\sum_{k=0}^{N-1} k^4 p[k]} = \sqrt{\sum_{j=0}^{N-1}(\Delta^2 x[j])^2} \qquad (6)$$

In the current circumstance, requiring the second and fourth derivative values of the sign diminishes the overall signal energy; therefore, we utilize a power change to standardize the scope of m_0, m_2 and m_4 to lessen the impact of commotion on all minutes based highlights, as in Eq. (7) [19]:

$$\begin{aligned} m_0 &= \frac{\overline{m}_0^\lambda}{\lambda} \\ m_2 &= \frac{\overline{m}_2^\lambda}{\lambda} \\ m_4 &= \frac{\overline{m}_4^\lambda}{\lambda} \end{aligned} \Bigg\} \qquad (7)$$

With a 0.1 empirical value. The first three variables' extracted features are then defined as [19]:

$$\begin{aligned} f_1 &= \log(m_0) \\ f_2 &= \log(m_0 - m_2) \\ f_4 &= \log(m_0 - m_4) \end{aligned} \Bigg\} \qquad (8)$$

a)   Sparseness:

This property quantifies the amount of energy in a vector and is expressed as an equation with only a few elements (9) [19]:

$$f_4 = \log\left(\frac{m_0}{\sqrt{m_0 - m_2}\sqrt{m_0 - m_4}}\right) \qquad (9)$$

Due to differentiation, m_2 and m_4 both equaling 0 and $\log(m_0/m_0)$, are vectors with entire components with a sparseness measurement that equals zero in which both m_2 and m_4 equal zero as well as $\log(m_0/m_0)$. In contrast, it should be more than zero for the remainder of sparsity levels [18].

b)   Irregularities Factors (IF):

The ratio of vertical zeroed intersections to peak numbers is known as a measure. According to the study [28], an arbitrary number of signals with upward zero-padded crossings (ZC) and multiple peaks (NP) could be entirely represented by their spectrum moments; the characteristic that corresponds to this is expressed as [19]:

$$f_5 = \frac{ZC}{NP} = \frac{\sqrt{\frac{m_2}{m_0}}}{\sqrt{\frac{m_4}{m_2}}} = \sqrt{\frac{m_2^2}{m_0 m_4}} = \frac{m_2}{\sqrt{m_0 m_4}} \qquad (10)$$

c)   Waveform Length Ratio (WL):

We express our WL features as the ratios of the first derivative's waveform lengths to the second derivative's waveform length. The waveform length attributes are defined as the sum of the absolutes signal derivative.

$$f_6 = \log\left(\frac{\sum_{j=0}^{N-1}|\Delta x|}{\sum_{j=0}^{N-1}|\Delta^2 x|}\right) \qquad (11)$$

The waveform length characteristic was crucial for the EMG activity classification [29]. The suggested WL features, on the contrary, build on previous work to provide an amplitude-invariant feature.

The last element, which are six recovered highlights for every EMG channel, are later separated in the direction of couple of vectors, as specified below:

$$f_i = \frac{-2a_i b_i}{a_i^2 + b_i^2} \quad i = 1, 2, 3, 4, 5, 6 \qquad (12)$$

The categorization process employs the attributes formulated by generated vectors f. These characteristics can be viewed as a form of EMG activity representation. In contrast to the famous sound spectral characteristics (a nonlinearly spectral of-a-spectral or, depending on implementation, the inversed Fast Fourier Transform(FFTs)of the logarithms of spectral [18].

2.2 Dimensionality reduction Spectral Regression (SR) method

Dimensionality reduction has been a significant challenge

in several data processing domains, like pattern recognition, machine learning, data mining, and information retrieval; Algorithms for supervised machine learning perform worse when confronted with a large number of features that are not necessary to predict the desired outcome (i.e., prediction accuracy).Extracting a few valuable features is one of the essential subjects in knowledge discovery, machine learning, pattern recognition, and computer vision. Using dimensionality reduction techniques is a common approach to solving this problem [30]. Traditional manifold learning methods, like the locally linear embedding, Laplacian Eigen map, and Isomap, provide training sample embedding results. To overcome the problem of out- of-sample extension, SR establishes a model of regression that can prevent the Eigen-decomposition of the dense matrices, which solves the difficulty of learning embedded functions [31]. The search for embedded functions that minimize fitness function in traditional spectral dimensionality reduction algorithms entails Eigen decomposition of the dense measures, having a high computational cost in time and memory. Instead of computing the density matrix of features, the SR algorithms employ the least-square approach to optimal projection direction, allowing them to learn significantly faster. To explore the structure of the underlying geometry and learn responses with given data, a G affinity graph with labeled and un labelled points was created. The embedding function is then realized using conventional regression using these responses[32].

2.3 Long Short-Term Memory (LSTM) concepts

Long Short-Term Memory (LSTM) is one type of neural network belonging to the RNN family that more accurately models chronologically based sequence and longly-ranged relationships than traditional RNN nets [33]. LSTM networks are a type of RNN created in response to the failure of RNNs. RNN is a network that works on the current input while also considering the previous output (feedback) and temporarily storing it in memory (short-term memory)[34]. LSTM has been constructed in such a way that it eliminates the vanishing gradient problem while leaving the training model unchanged. Long temporal gaps are bridged in specific situations using LSTMs, which can also manage distributed representations, noise, and continual values. Additionally, no requirement to preserve a limited number of cases from the beginning with LSTMs, as in Hidden Markova Model (HMM). LSTMs offer input and output biases in addition to a number of other parameters like learning rates. Consequently, no accurate modification is needed. LSTM minimizes the intricacy of updating each weight to $O(1)$, like Back Propagation Through Time (BPTT), which is an advantage [35].

2.3.1 Exploding and vanishing gradients problem
The fundamental objective of the training process is to reduce the amount of losses regarding cost or error seen in the output. We calculate the gradient, or loss, for a given set of weights, make necessary adjustments and repeat until we have the best set of weights with the least amount of loss. The term "backtracking" refers to the process of going backwards [36]. Occasionally, the gradient is so small that it is nearly unnoticeable. It is worth noting that specific parts in subsequent levels influence the growth of layers. The gradient that is obtained will be even less if these parts are small (<1). The scaling effect is the name for this process. A tiny number

between 0.1 and 0.001 produces a smaller value when the learning rate is multiplied by this gradient [37]. As a result, the weight changes are minor, and the output is nearly identical to previously. Similarly, if the gradients are very large due to high component values, the weights are changed to a value that is not ideal. The problem of bursting gradients is a term used to describe this situation. To eliminate this scaling impact, the neural network unit was re-built with a one-to-one scaling factor. Several gating units known as LSTM were then added to the cell [38].

2.4 Linear Discriminate Analysis (LDA) method

The goal of LDA is to create a new variable by combining the basic prediction methods. In order to do this, the predefined bunches in the new variables are enhanced to provide clearer distinctions between them. The objective is to join the forecast scores into a solitary composite variable named the discriminant scores. This is a data compression procedure that diminishes the p-layered indicators to one layered line. Each class should have a typical distribution of discriminant scores at the end of the cycle. The overlapping degree of the discriminants scores distribution could be utilised to evaluate the technique's effectiveness in practice. The following discriminant function is used to obtain discriminant scores [39]:

$$D = w_1 Z_1 + w_2 Z_2 + w_3 Z_3 + \cdots w_p Z_p \qquad (13)$$

As a result, discriminant scores are weighted using linear combinations of predictors. To maximize the variations in mean discriminant scores between classes, weights are calculated. In general, weights will be higher for predictors with large differences between class means, while weights will be lower for predictors with similar class means [40].

3. THE PROPOSED RECOGNITION SYSTEM

The proposed work scheme for Recognition of different shoulder motions for Prosthesis Control by Time-Dependent Power Spectrum includes signals Pre-Processing (cross-validation, segmentation) stage, features extraction, dimensionality reduction, and classification stages. Cross-validation of training and test data, followed by segmentation with an overlap window size, are utilized to pre-propose the provided signals, as shown in Figure 2. After that, features extraction using Time-Dependent Power Spectrum Descriptor (TD-PSD) by measuring six statistical functions for each extracted dimension are presented. Following the SR dimension reduction presentation, the LDA and LSTM classifiers are finally used to identify seven other shoulder girdle motions for prosthesis control. These steps are described in further detail in the subsections that follow:

3.1 Input signal

This section explains the basic concepts behind the details of data collection used by Sharba et al. [21]. For the classification of shoulder girdle motions, information was collected from four amputee subjects and six subjects with intact limbs, a set of seven movements was chosen: downward rotation, depression, upward rotation, elevation, protraction, retraction, and rest. five EMG channels were recorded in the

data. Furthermore, a 3-axis accelerometer sensor (ADXL335) was mounted on the top of the shoulder to give three accelerometers (Acc) channels. Similar to the EMG sensor, the data was captured using the USB 6009 acquisition system and transmitted at a rate of 1000 Hz per second. Its scale range was 3g, its bandwidth ranged from 0.5 to 1600 Hz, and its power supply requirements were 1.8 to 3.6 V [21]. In the Figure 3(a) the locations of the recorded five channels of the EMG signal and three Acc channels are shown for an intact-limbed subject, and the same channels sites for the amputee subject are shown in Figure 3(b).
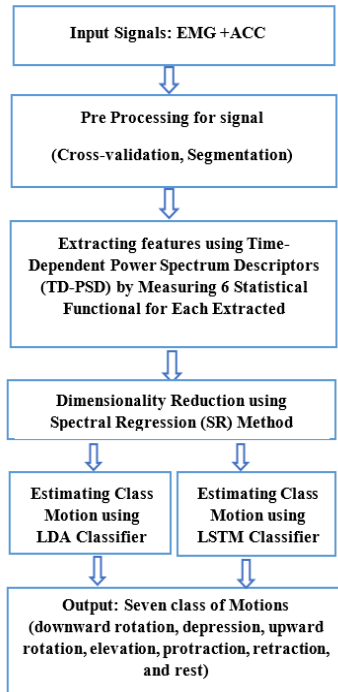

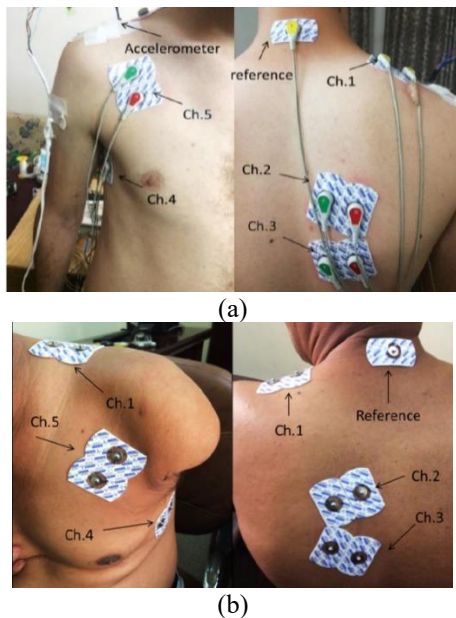**Figure 2.** The general design of the proposed work scheme

(a)

(b)

Figure 3. (a) Demonstrating a sample of the precise electrode placements for a person with intact limbs; (b) Shows an illustration of the precise electrode placement for the amputee subject's muscles

3.2 Pre-processing for signal

For the training and testing phases of machine learning, sampling is crucial. An unbalanced data sampling can directly affect the results of training and testing. Consequently, the entire dataset should be represented by both the training and test sets of data. The success rate is primarily affected by how much training and testing is conducted. In the literature, different training test ratios have been employed [41]. Cross-validation with one trail left out was used in this study. The final individual trail was used to test the classifier and determined the classification error rate after seven trails for each fold were used to train the classifier. We used this procedure eight times in total to determine the average error rates over the eight runs.

a) Cross- validation

A machine-learning model's performance can be assessed and tested using the cross-validation (CV) technique (or accuracy). It requires setting aside a section of a dataset on which the model has not yet been trained. On this sample, the model is then evaluated to see how well it performs. However, it is employed to avoid overfitting a model, particularly when there is a scarcity of data. It's also referred to as out-of-sample testing or rotation estimation, and it's most frequently utilized when the model's objective is prediction [27]. The standard method is as follows:

1. Shuffle the dataset at random.
2. Split up the data into a total of k groups
3. for each unique group:
- The group should be used as a holdout or test data set, Moreover, the other groups should be used as Training Data sets.
- On the training set, put together a model, and then test it on the test set.
- The model is discarded, but the evaluation result is kept.
4. Use the sample of model evaluation ratings to summarize the model's performance.

It is crucial that every observation in the data sample is given a specific category and stays there throughout the process. This implies that each sample has an equal probability of being utilized in the hold-out set and that the model will be trained k times [42]. Cross-validation was applied, as shown in Figure 4.
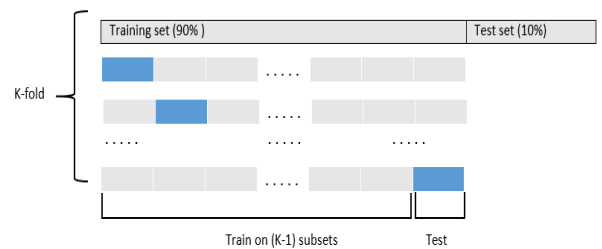

Figure 4. Examples of K-fold cross-validation dataset partitioning

b) Segmentation

The raw signals are gathered at sample rates of 1 kHz. 150 ms for the windowing size and 50 ms for the windowing increment, data segmentation was also carried out using an overlapping segmentation approach. EMG signals from five channels are seen in Figure 5, and the three channels of the Acc. Signals are shown in Figure 6.

CH1

CH2

CH3

CH4

CH5
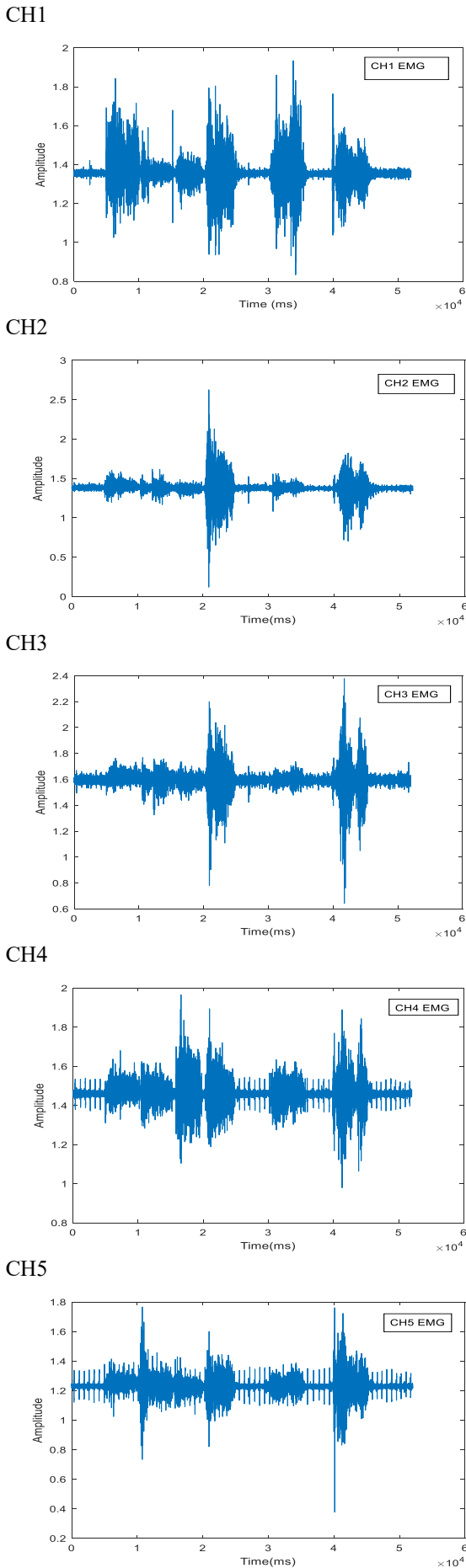
Figure 5. Examples of EMG data (5 Channels) in the pre-processing condition

CH6

CH7

CH8
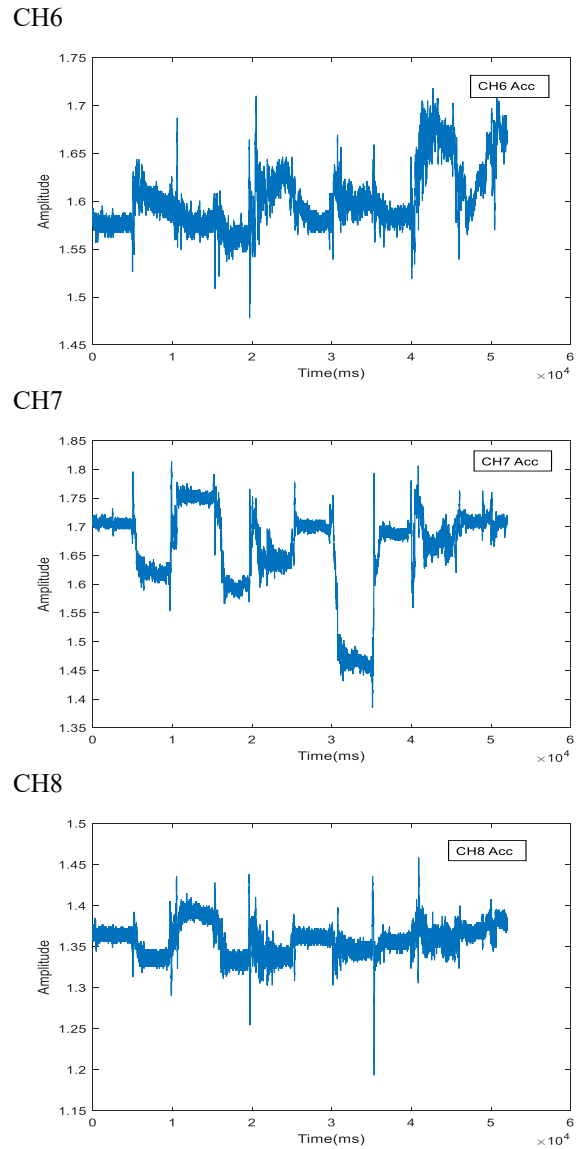
Figure 6. Examples of 3-axis accelerometer sensor data (3 channels) in pre-processing condition

3.3 Time-Dependent Power Spectrum Descriptors (TD-PSD) based features extraction

Each channel's data is initially split into frames with a windowing size of 150 ms and an overlap of 50 ms to guarantee the durability of each frame. Six feature groups are then generated from the channels (i.e., 8-dimensions), including the Root squared zero-order moment ($\bar{m}_0$), Root squared second ($\bar{m}_2$) and fourth-order moments ($\bar{m}_4$) (i.e., 16-dimension with first and second derivative values), Sparseness (8-dimension), Irregularity Factor (i.e., F1 with 8-dimension), Waveform Length Ratio (WL), (i.e., 8-dimension). The extracted features have 48 total dimensions.

4. DIMENSIONALITY REDUCTION USING SPECTRAL REGRESSION (SR) METHOD

SR is the complex linear time with respect to the number of features and data samples. In addition to the data matrix, it only requires very little additional memory. As a result, scaling SR to large, high-dimensional data sets is simple. The benefits of using SR rather than just applying LDA directly are evident

from the computational complexity analysis [43].

Recently, spectral techniques have become a potent tool for manifold learning and dimensionality reduction. These techniques make the low dimensional structure of the high dimensional data visible by using the data found in the eigenvectors of a data affinity (item-item similarity) matrix [44]. This article introduces the spectral regression framework for dimension reduction (SR). The challenge presented by SR is how to learn the modulation function within a regression framework without dielectricizing dense matrices. Additionally, since regression is a fundamental building block, various regulator types can be easily incorporated into our crafting framework, making it more adaptable. There are three conditions in which SR can be done: supervised, unsupervised, and semi-supervised. It can effectively use labelled and unlabelled points to find the data's intrinsic characteristic structure [45].

The input parameters to this function are a data matrix (feature training, feature testing) A sample vector, or Struct value in Matlab, is contained in each row of data. Options for the fields include a column vector of label information for each data point (gnd), as well as how many dimensions there are (Reduced Dim) Reduced Dim=c-1 if (gnd) is given, where c represents the number of classes, and on the otherwise Default Reduced Dim equal thirty [46].

5. MOTION CLASSIFICATION METHODS

The accuracy and selection time of various classifier variants were examined for this study using two different classification methods, as detailed in the following subsections.

A. Estimating class motion using LDA classifier

The LDA classification framework, which was applied in this study, assumes gaussian distribution of the data. The discriminant function for the LDA is expressed by equation (18).

B. Estimating class motion using LSTM classifier

The proposed LSTM model has N hidden layers and 192 cell units to categorize seven hand and wrist movements. A fully connected layer follows these layers. With a mini-batch size of 170, an Adam optimizer-learning rate of 0.001, a keep probability of 0.25, dropout regularization, and 30 iterations, the LSTM model was trained and verified. Gradient clipping was implemented to enhance training by preventing gradient explosions during back propagation.

6. EXPERIMENTAL RESULTS

6.1 Experimental setup

Using the overlapping segmentation method, the data was first divided into 50 ms increments with a window size of 150 ms. In addition, a proposed model, which has been trained over all the available data (10 subjects) using an 8-fold cross-subject validation scheme. The remaining individual trails were used to test classifiers and calculate classification error rates. This procedure has been repeated eight times. After completing the eight runs, the average error rate for those eight trials was calculated.

6.2 Performance evaluation

The suggested model's performance is assessed in this study using the classification error ratio (CER), which is derived using Eq. (19):

$$\text{Err} = (1-(\text{sum (YPred==YTest). /numel (YTest)}))*100 \tag{19}$$

where, model predicted and YPred and YTest denote experimental feature testing, respectively.

6.3 Testing error using based on LDA classifier

TD-PSD-like features, including the square root of zero order moments, second and fourth square root moments, variance, irregularity factor (IF), and wavelength ratio (WL), were used in the first experiment. In addition, eight different values were tested for each fold (cross-validation). The average test error achieved for each SR (dimensionality reduction) is calculated based on the objective value using an LDA classifier, as shown in Figure 7. In the present experiments, the experiment was conducted on six subjects with healthy limbs with average classification error from 9.48% to 15.86%.
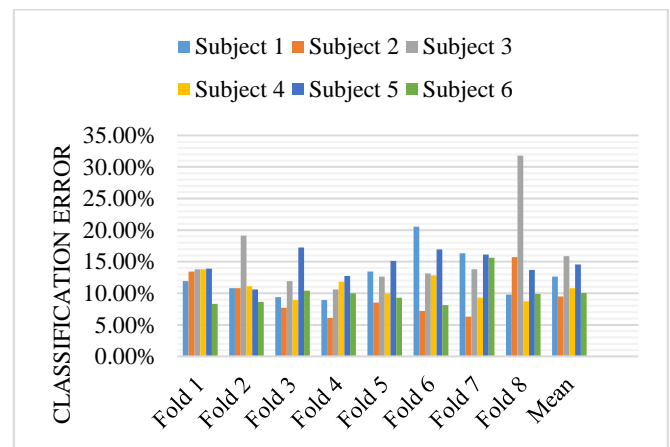

Figure 7. Classification error for six healthy subjects with LDA classifier
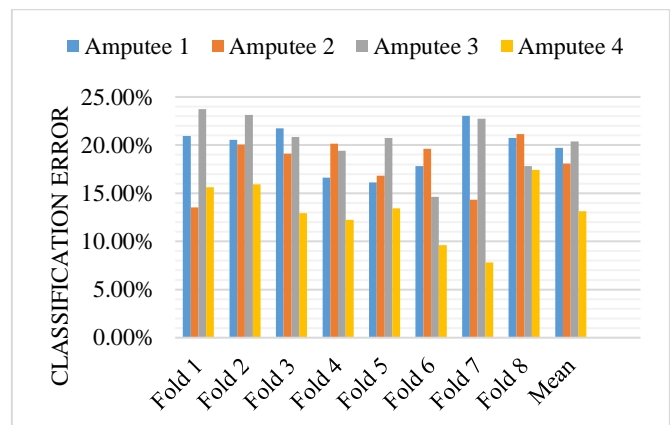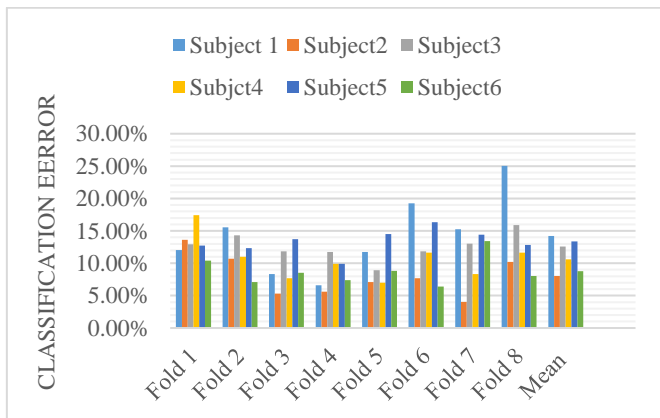

Figure 8. Classification error for four amputees with LDA classifier

The second experiment is conducted using the group of features as TD-PSD. In addition; eight different values for
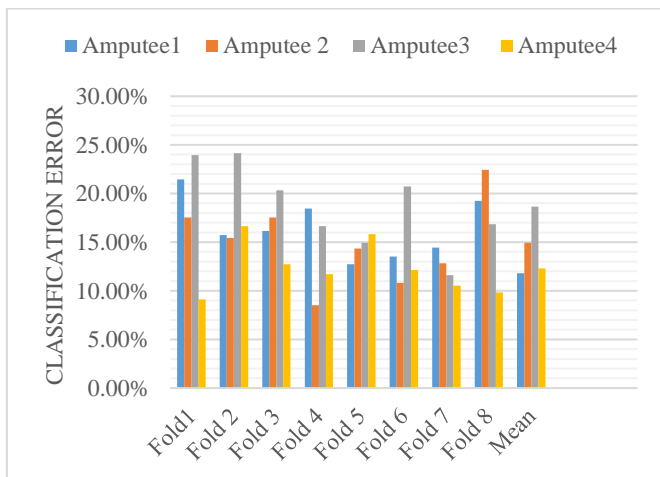
each fold (cross-validation) have been tested. The average test error achieved for each SR (dimensionality reduction) is calculated based on the objective value using an LDA classifier, as shown in Figure 8. In the present experiments, the experiment was conducted on four subjects with amputee subjects with average classification error from 13.12% to 20.39%.

6.4 Testing error using based on LSTM classifier

A feature set similar to TD-PSD was used in the third experiment, including the square roots of zero order moments, second and fourth square root moments, variance, irregularity factor (IF), and wavelength ratio (WL). In addition, eight different values were tested for each fold (cross-validation). The average test error achieved for each SR (dimensionality reduction) is calculated based on the objective value using an LSTM classifier, as shown in Figure 9. In the present experiments, the experiment was conducted on six subjects with healthy limbs with average classification error from 8.04% to 14.22%.

Figure 9. Classification error for six intact subjects with LSTM classifier
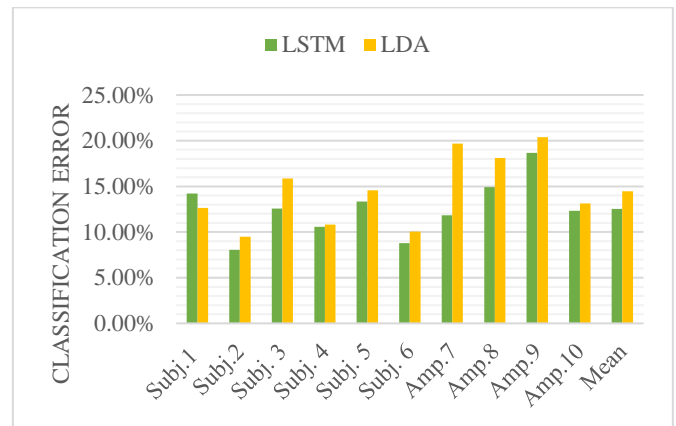

Figure 10. Classification error for four amputee subjects with LSTM classifier

Again, the fourth experiment is conducted using the group of features as TD-PSD. In addition; eight different values for each fold (cross-validation) have been tested. The average test error achieved for each SR (dimensionality reduction) is calculated based on the objective value using an LDA

classifier, as shown in Figure 10. In the present experiments, the experiment was conducted on four subjects with amputee subjects with average classification error from 11.82% to 18.65%.

The last experiment compared LSTM and LDA classifiers on the achieved testing error for models based on TD-PSD feature extraction with SR dimensionality reduction. Figure 11 illustrates how the LSTM and LDA classifier types affect classification accuracy, as shown by the fact that using the LSTM classifier causes a reduction in the value of classification error. LDA classifier's average classification error is 14.47%, while LSTM classifier's average classification error is 12.52%.

Figure 11. Classification error for 10 subjects with LSTM and LDA classifier

7. DISCUSSION

The mean classification errors for 10 subjects with intact-limbs of 11.24% and amputees of 14.43% dispalyed in Figure 11, the results showed that the LSTM classifier outperformed the LDA classifier for the categorization of the seven classes of the shoulder girdle. The classification error for amputees was equal to 17.83% and was calculated as 12.23% for subjects with intact limbs. According to Figure 7, the second subject had lower mean classification errors than the other five subjects when employing EMG, an accelerometer, and an LDA classifier to classify six intact-limbed participants. Figure 8 demonstrates that the mean classification error of the fourth amputee subject is lower than that of the other three amputee subjects. Figure 9 and Figure 10 display, the mean classification errors for six subjects with intact limbs and four amputee subjects, respectively, using the LSTM classifier. Less classification applies to the subject with intact limbs (Subject 2) and the amputee (Amputee 1).

The most accurate classification of shoulder girdle motions was determined in the final study in this paper. The outcomes for subjects with intact limbs and amputees are shown in Figure 11. Some intriguing findings came from looking at the LDA and LSTM classifiers. When using LSTM, the classification errors were reduced from 14.47% for LDA to 12.52%, which is comparable to a usable PR system.

8. CONCLUSIONS

This study examined seven different types of shoulder

girdle motions in high-level upper-limb amputees using accelerometer and EMG signals. These results will help researchers decide whether shoulder girdle motions are suitable for upper-limb amputees using PR systems as non-invasive and natural control signals. The regions of interest help to concentrate Time-Dependent Power Spectrum Descriptors (TD-PSD) feature extraction with SR dimensionality reduction for EMG and accelerometer signal based conventional machine learning techniques such as LDA classifier and Deep Learning approaches such as LSTM with signal fusion to improve the efficiency of hand and wrist motion control. The experimental findings showed that the proposed Pattern Recognition system could identify seven shoulder girdle motions with a classification testing error of 12.52% for six subjects with intact limbs and four amputees using SR dimensionality reduction with LSTM classifier and 14.47% for the same feature extraction method and dimensionality reduction with LDA classifier. This reflects the nature of LSTM models that ability to capture long-term dependency and enhanced expansive power. In contrast, the LDA classifier works in less manner. However, as the number of features increases, the task becomes more complex. We recommend transferring the movements of the prosthetic hand to the shoulder girdle in order to control a prosthetic arm in the future and improve everyday life for those with severe upper-limb amputees.

REFERENCES

[1] Kuiken, T.A., Li, G., Lock, B.A., Lipschutz, R.D., Miller, L.A., Stubblefield, K.A., Englehart, K.B. (2009). Targeted muscle reinnervation for real-time myoelectric control of multifunction artificial arms. Jama, 301(6): 619-628. https://doi.org/10.1001/jama.2009.116

[2] Englehart, K., Hudgins, B. (2003). A robust, real-time control scheme for multifunction myoelectric control. IEEE Transactions on Biomedical Engineering, 50(7): 848-854. https://doi.org/10.1109/TBME.2003.813539

[3] Merletti, R., Parker, P.J. (Eds.). (2004). Electromyography: Physiology, Engineering, and Non-Invasive Applications. John Wiley & Sons.

[4] Hudgins, B., Parker, P., Scott, R.N. (1993). A new strategy for multifunction myoelectric control. IEEE Transactions on Biomedical Engineering, 40(1): 82-94. https://doi.org/10.1109/10.204774

[5] Grushko, S., Spurný, T., Černý, M. (2020). Control methods for transradial prostheses based on remnant muscle activity and its relationship with proprioceptive feedback. Sensors, 20(17): 4883. https://doi.org/10.3390/s20174883

[6] Nsugbe, E. (2021). Brain-machine and muscle-machine bio-sensing methods for gesture intent acquisition in upper-limb prosthesis control: A review. Journal of Medical Engineering & Technology, 45(2): 115-128. https://doi.org/10.1080/03091902.2020.1854357

[7] Fougner, A., Stavdahl, Ø., Kyberd, P.J., Losier, Y.G., Parker, P.A. (2012). Control of upper limb prostheses: Terminology and proportional myoelectric control—A review. IEEE Transactions on Neural Systems and Rehabilitation Engineering, 20(5): 663-677. https://doi.org/10.1109/TNSRE.2012.2196711

[8] Bertani, R., Melegari, C., De Cola, M.C., Bramanti, A., Bramanti, P., Calabrò, R.S. (2017). Effects of robot-assisted upper limb rehabilitation in stroke patients: A systematic review with meta-analysis. Neurological Sciences, 38: 1561-1569. https://doi.org/10.1007/s10072-017-2995-5

[9] Nabian, M., Nouhi, A., Yin, Y., Ostadabbas, S. (2017). A biosignal-specific processing tool for machine learning and pattern recognition. In 2017 IEEE Healthcare Innovations and Point of Care Technologies (HI-POCT), Bethesda, MD, USA, pp. 76-80. https://doi.org/10.1109/HIC.2017.8227588

[10] Parajuli, N., Sreenivasan, N., Bifulco, P., Cesarelli, M., Savino, S., Niola, V., Esposito, D., Hamilton, T.J., Naik, G.R., Gunawardana, U., Gargiulo, G.D. (2019). Real-time EMG based pattern recognition control for hand prostheses: A review on existing methods, challenges and future implementation. Sensors, 19(20): 4596. https://doi.org/10.3390/s19204596

[11] Boostani, R., Moradi, M.H. (2003). Evaluation of the forearm EMG signal features for the control of a prosthetic hand. Physiological Measurement, 24(2): 309. https://doi.org/10.1088/0967-3334/24/2/307

[12] Oskoei, M.A., Hu, H. (2007). Myoelectric control systems—A survey. Biomedical Signal Processing and Control, 2(4): 275-294. https://doi.org/10.1016/j.bspc.2007.07.009

[13] Zardoshti-Kermani, M., Wheeler, B.C., Badie, K., Hashemi, R.M. (1995). EMG feature evaluation for movement control of upper extremity prostheses. IEEE Transactions on Rehabilitation Engineering, 3(4): 324-333. https://doi.org/10.1109/86.481972

[14] Khushaba, R.N., Shi, L., Kodagoda, S. (2012). Time-dependent spectral features for limb position invariant myoelectric pattern recognition. In 2012 International Symposium on Communications and Information Technologies (ISCIT), Gold Coast, QLD, Australia, pp. 1015-1020. https://doi.org/10.1109/ISCIT.2012.6380840

[15] Matsumura, Y., Fukumi, M., Mitsukura, Y. (2006). Hybrid EMG recognition system by MDA and PCA. In The 2006 IEEE International Joint Conference on Neural Network Proceedings, Vancouver, BC, Canada, pp. 5294-5300. https://doi.org/10.1109/IJCNN.2006.247285

[16] Khushaba, R.N., Al-Jumaily, A., Al-Ani, A. (2007). Novel feature extraction method based on fuzzy entropy and wavelet packet transform for myoelectric control. In 2007 International Symposium on Communications and Information Technologies, Sydney, NSW, Australia, pp. 352-357. https://doi.org/10.1109/ISCIT.2007.4392044

[17] Yan, Z., Wang, Z., Xie, H. (2008). Joint application of rough set-based feature reduction and fuzzy LS-SVM classifier in motion classification. Medical & Biological Engineering & Computing, 46: 519-527. https://doi.org/10.1007/s11517-007-0291-x

[18] Khushaba, R.N., Takruri, M., Miro, J.V., Kodagoda, S. (2014). Towards limb position invariant myoelectric pattern recognition using time-dependent spectral features. Neural Networks, 55: 42-58. https://doi.org/10.1016/j.neunet.2014.03.010

[19] Al-Timemy, A.H., Khushaba, R.N., Bugmann, G., Escudero, J. (2015). Improving the performance against force variation of EMG controlled multifunctional upper-limb prostheses for transradial amputees. IEEE Transactions on Neural Systems and Rehabilitation Engineering, 24(6): 650-661. https://doi.org/10.1109/TNSRE.2015.2445634

[20] Khushaba, R.N., Al-Timemy, A.H., Al-Ani, A., Al-Jumaily, A. (2017). A framework of temporal-spatial descriptors-based feature extraction for improved myoelectric pattern recognition. IEEE Transactions on Neural Systems and Rehabilitation Engineering, 25(10): 1821-1831. https://doi.org/10.1109/TNSRE.2017.2687520

[21] Sharba, G.K., Wali, M.K., Al-Timemy, A.H. (2020). Wavelet-based feature extraction technique for classification of different shoulder girdle motions for high-level upper limb amputees. International Journal of Medical Engineering and Informatics, 12(6): 609-619. https://doi.org/10.1504/IJMEI.2020.111042

[22] Xu, Y., Liu, X., Cao, X., et al. (2021). Artificial intelligence: A powerful paradigm for scientific research. The Innovation, 2(4): 100179. https://doi.org/10.1016/j.xinn.2021.100179

[23] Mikolov, T., Joulin, A., Chopra, S., Mathieu, M., Ranzato, M.A. (2014). Learning longer memory in recurrent neural networks. arXiv preprint arXiv:1412.7753. https://doi.org/10.48550/arXiv.1412.7753

[24] Qiao, M., Li, H. (2020). Application of PCA-LSTM model in human behavior recognition. Journal of Physics: Conference Series, 1650(3): 032161. https://doi.org/10.1088/1742-6596/1650/3/032161

[25] Dao, T.T. (2019). From deep learning to transfer learning for the prediction of skeletal muscle forces. Medical & Biological Engineering & Computing, 57: 1049-1058. https://doi.org/10.1007/s11517-018-1940-y

[26] Chen, Y., Yu, S., Ma, K., Huang, S., Li, G., Cai, S., Xie, L. (2019). A continuous estimation model of upper limb joint angles by using surface electromyography and deep learning method. IEEE Access, 7: 174940-174950. https://doi.org/10.1109/ACCESS.2019.2956951

[27] Hjorth, B. (1970). EEG analysis based on time domain properties. Electroencephalography and clinical neurophysiology, 29(3): 306-310. https://doi.org/10.1016/0013-4694(70)90143-4

[28] Dirlik, T. (1985). Application of computers in fatigue analysis. PhD thesis, University of Warwick. http://go.warwick.ac.uk/wrap/2949

[29] Zecca, M., Micera, S., Carrozza, M.C., Dario, P. (2002). Control of multifunctional prosthetic hands by processing the electromyographic signal. Critical Reviews™ in Biomedical Engineering, 30(4-6): 459-485. https://doi.org/10.1615/CritRevBiomedEng.v30.i456.80

[30] Aziz, R., Verma, C.K., Srivastava, N. (2017). Dimension reduction methods for microarray data: A review. AIMS Bioeng, 4(1): 179-197. https://doi.org/10.3934/bioeng.2017.2.179

[31] Dong, Y. (2021). A brief review of linear sufficient dimension reduction through optimization. Journal of Statistical Planning and Inference, 211: 154-161. https://doi.org/10.1016/j.jspi.2020.06.006

[32] Zenil, H., Kiani, N.A., Adams, A., Abrahão, F.S., Rueda-Toicen, A., Zea, A.A., Tegnér, J. (2018). Minimal algorithmic information loss methods for dimension reduction, feature selection and network sparsification. arXiv preprint arXiv:1802.05843. https://doi.org/10.48550/arXiv.1802.05843

[33] Lipton, Z.C., Kale, D.C., Elkan, C., Wetzel, R. (2015). Learning to diagnose with LSTM recurrent neural networks. arXiv preprint arXiv:1511.03677. https://doi.org/10.48550/arXiv.1511.03677

[34] Lipton, Z.C., Berkowitz, J., Elkan, C. (2015). A critical review of recurrent neural networks for sequence learning. arXiv preprint arXiv:1506.00019. https://doi.org/10.48550/arXiv.1506.00019

[35] Mikami, A. (2016). Long Short-Term Memory recurrent neural network architectures for generating music and japanese lyrics. Thesis, Boston College.

[36] Brownlee, J. (2019). Loss and loss functions for training deep learning neural networks. Machine Learning Mastery, 23: 22.

[37] Uranga, A., Drela, M., Hall, D.K., Greitzer, E.M. (2018). Analysis of the aerodynamic benefit from boundary layer ingestion for transport aircraft. AIAA Journal, 56(11): 4271-4281. https://doi.org/10.2514/1.J056781

[38] Liu, M., Chen, L., Du, X., Jin, L., Shang, M. (2021). Activated gradients for deep neural networks. IEEE Transactions on Neural Networks and Learning Systems, 34(4): 2156-2168. https://doi.org/10.1109/TNNLS.2021.3106044

[39] Buk, A A.Y., Wali, M.K., Al-Timemy, A.H., Raoof, K. (2020). Hand gesture recognition using mechanomyography signal based on LDA classifier. In IOP Conference Series: Materials Science and Engineering, 881(1): 012125. https://doi.org/10.1088/1757-899X/881/1/012125

[40] Subasi, A., Gursoy, M.I. (2010). EEG signal classification using PCA, ICA, LDA and support vector machines. Expert Systems with Applications, 37(12): 8659-8666. https://doi.org/10.1016/j.eswa.2010.06.065

[41] Uçar, M.K., Nour, M., Sindi, H., Polat, K. (2020). The effect of training and testing process on machine learning in biomedical datasets. Mathematical Problems in Engineering, 2020: 2836236. https://doi.org/10.1155/2020/2836236

[42] Fang, X., Li, H., Zhang, S.R., Wang, X.H., Wang, C., Luo, X.C. (2022). A combined finite element and deep learning network for structural dynamic response estimation on concrete gravity dam subjected to blast loads. Defence Technology. https://doi.org/10.1016/j.dt.2022.04.012

[43] Cai, D. (2009). Spectral regression: A regression framework for efficient regularized subspace learning. University of Illinois at Urbana-Champaign.

[44] Cai, D., He, X., Han, J. (2007). Spectral regression for dimensionality reduction. University of Illinois at Urbana-Champaign.

[45] Law, C.W., Zeglinski, K., Dong, X., Alhamdoosh, M., Smyth, G.K., Ritchie, M.E. (2020). A guide to creating design matrices for gene expression experiments. F1000Research, 9: 1444. https://doi.org/10.12688/f1000research.27893.1

[46] Cai, D., He, X., Han, J. (2007). SRDA: An efficient algorithm for large-scale discriminant analysis. IEEE Transactions on Knowledge and Data Engineering, 20(1): 1-12. https://doi.org/10.1109/TKDE.2007.190669